

Journal of Materials Chemistry B

Accepted Manuscript



This is an *Accepted Manuscript*, which has been through the Royal Society of Chemistry peer review process and has been accepted for publication.

Accepted Manuscripts are published online shortly after acceptance, before technical editing, formatting and proof reading. Using this free service, authors can make their results available to the community, in citable form, before we publish the edited article. We will replace this *Accepted Manuscript* with the edited and formatted *Advance Article* as soon as it is available.

You can find more information about *Accepted Manuscripts* in the [Information for Authors](#).

Please note that technical editing may introduce minor changes to the text and/or graphics, which may alter content. The journal's standard [Terms & Conditions](#) and the [Ethical guidelines](#) still apply. In no event shall the Royal Society of Chemistry be held responsible for any errors or omissions in this *Accepted Manuscript* or any consequences arising from the use of any information it contains.

Cite this: DOI: 10.1039/c0xx00000x

www.rsc.org/xxxxxx

ARTICLE TYPE

Hollow hydroxyapatite/polyelectrolyte hybrid microparticles with controllable size, wall thickness and drug delivery property

Jing Wei, Jun Shi*, Qiong Wu, Liu Yang and Shaokui Cao*

Received (in XXX, XXX) Xth XXXXXXXX 20XX, Accepted Xth XXXXXXXX 20XX

DOI: 10.1039/b000000x

Hybrid hydroxyapatite (HAP) microparticles with a hollow HAP core and chitosan/hyaluronic acid (CHI/HA) multilayer shell had been fabricated via hydrothermal method and the layer-by-layer (LbL) self-assembly technique. Depending on the hydrothermal reaction time, the thickness of the HAP shell could be controlled and the size of the hybrid hollow microparticles varied between 850 nm and 2 μm . The size and HAP shell thickness would significantly affect the drug release property of the resulting hybrid microparticles. The DOX release results demonstrated that CHI/HA multilayers could potentially assuage the initial burst release of drug from porous HAP matrix because the polymer multilayer shell acted as a barrier to control the in-and-out of the drug. In addition, the drug release of hollow hybrid HAP microparticles was pH-dependent because of the different electrostatic interaction in the CHI/HA multilayers at different pH values and the dissolution of HAP hollow core at acid condition. The present paper provides a facile and green route to fabricate hierarchical hybrid drug carrier with controllable size, wall thickness and drug release property by combining natural polyelectrolyte and hollow HAP microparticles, which is highly attractive for controllable drug delivery.

Keywords: Hydroxyapatite; Polyelectrolyte; Hollow microparticles; Controllable morphology; Drug delivery

1. Introduction

Inorganic/organic hybrid microparticles have been widely employed in drug or gene delivery area due to its outstanding advantages of hierarchical structures, integrate and excellent mechanical strength.¹⁻⁴ Hydroxyapatite ($\text{Ca}_{10}(\text{PO}_4)_6(\text{OH})_2$, HAP), as the major constituents of inorganic components of bone textures in the human body, has been widely employed in inorganic/organic hybrid drug carrier area for its good biocompatibility, biodegradability and biological activity.⁵⁻⁹ Currently, a number of studies have focused on hollow HAP (H-HAP) microparticles, which show relatively lower density, higher specific surface area and higher capacity for drug loading application.¹⁰⁻¹³ Among various approaches of preparing H-HAP microparticles¹⁴⁻¹⁶, the template method is the most common one, which is based on a core template to build sphere architectures and followed by core dissolution.¹⁷⁻²⁰ Guo et al. prepared a series of mesoporous HAP drug delivery carriers via the hydrothermal reaction, which exhibited high specific surface area and drug loading capacity.²¹⁻²³ However, a rapid initial burst release was often observed for H-HAP microparticles in the above studies.^{24,25} Moreover, there have been few reports on the regulation of the size and HAP shell thickness for these H-HAP microparticles. Therefore, it is a great challenge to prepare H-HAP-based drug carriers with controllable morphology and drug release property via simple and environmentally friendly

method.

Combining the H-HAP microparticles with polyelectrolyte multilayers is a good method to get rid of the rapid initial burst release of HAP-based drug carriers.^{26,27} Layer-by-layer (LbL) self-assembly technique is a well-established technique for fabricating polyelectrolyte multilayers and then incorporating the multilayers with porous inorganic microparticles, which has been widely employed in the preparation of inorganic/organic hybrid nano-/micro-particles.²⁸⁻³¹ In order to achieve controllable morphology and drug delivery property, an innovative HAP-based hybrid drug carrier with the controllable size, wall thickness and drug release property has been proposed in this work. Hyaluronic acid (HA) and chitosan (CHI) have been selected as the polyelectrolytes for LbL technique. HA is linear weak polyacid ($\text{pK}_a = 3.0$), which is composed of 2-acetamide-2-deoxy- β -D-glucose and β -D-glucuronic acid residues linked by alternate (1-3) and (1-4) glycosidic bonds.³²⁻³⁴ Compared with other natural polymers, HA has been widely used in biomedical area, especially in ophthalmic area, because it has better biodegradability, biocompatibility and lower toxicity.^{35,36}

In the present paper, the H-HAP/polyelectrolyte hybrid microparticles with a hollow HAP core and polymer multilayer shell have been prepared by the LbL technique as illustrated in Fig. 1. Carbonated HAP microparticles were obtained via hydrothermal and dissolution-precipitation reaction using PSS-doped vaterite CaCO_3 as template.^{26,27} The size and wall

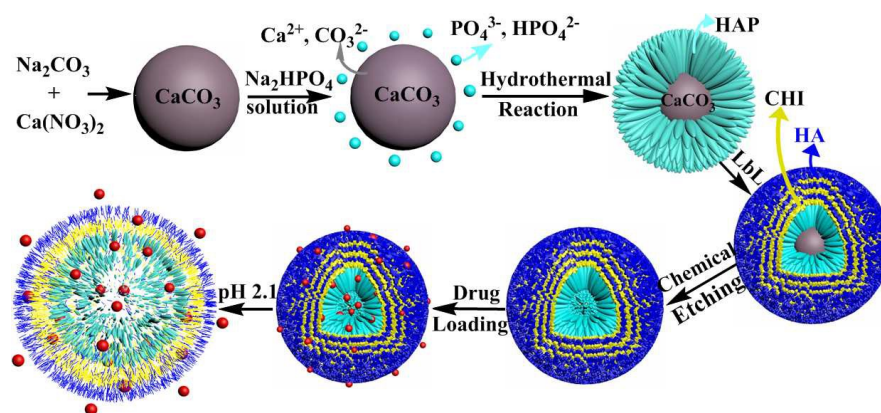


Fig. 1 Schematic illustration of the fabrication of H-HAP/CHI/HA hybrid microparticles.

thickness of hollow HAP microparticles were controlled by adjusting the hydrothermal reaction time as shown in Fig. 2. In the following step, PSS-doped HAP microparticles could easily incorporate with CHI and HA to form multilayer-coated HAP microparticles. Finally, the hollow HAP/polyelectrolyte (H-HAP/CHI/HA) hybrid microparticles were obtained by removing the CaCO_3 cores with acetic acid.^{26,27}

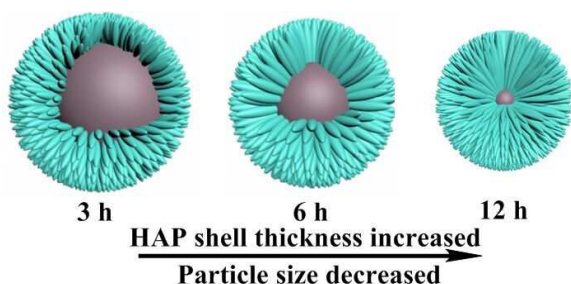


Fig. 2 Schematic illustration of HAP microparticles with different size and wall thickness prepared by different hydrothermal reaction time.

The objective of this study was to obtain hollow HAP/polyelectrolyte hybrid microparticles with controllable size, wall thickness and drug release property. The results demonstrated that the thickness of the hollow HAP shell could be controlled via the adjustment of hydrothermal reaction condition, and the size of the resulting hybrid microparticles varied between 850 nm and 2 μm . Doxorubicin hydrochloride (DOX) release results revealed that CHI/HA multilayers could assuage the initial burst release of DOX from porous HAP matrix because of the introduction of compact polyelectrolyte barriers. In addition, thanks to the dissolution of HAP and weakening of the electrostatic force between polyelectrolytes in the acidic media, the DOX release exhibited distinguished pH-dependent property.²⁶ The present paper provides a facile and green route to fabricate hierarchical environmentally friendly drug carrier with controllable size, wall thickness and drug release property by combining natural polyelectrolyte and hollow HAP microparticles, which is highly attractive for drug delivery area.

2. Experimental section

2.1 Materials

Sodium poly(styrenesulfonate) (PSS, $M_w = 70\,000$, Alfa Organics, China), calcium nitrate ($\text{Ca}(\text{NO}_3)_2$, Tianjin Chemical Reagent Factory, China), sodium carbonate (Na_2CO_3 , Tianjin Hengxing Chemical, China), disodium hydrogen phosphate dodecahydrate ($\text{Na}_2\text{HPO}_4 \cdot 12\text{H}_2\text{O}$, Zhiyuan Reagent Co. China), chitosan (CHI, with a 85% degree of deacetylation and a viscosity of 30 cps, Jinan Haidebei Marine Bioengineering Co. China), hyaluronic acid (HA, $M_w = 1.68 \times 10^5$) and doxorubicin hydrochloride (DOX, Beijing Huafenglianbo Chemical, China) were all analytical reagents and used as received. The water used in all experiments was triple-distilled.

2.2 Preparation of HAP microparticles with a CaCO_3 core

CaCO_3 microparticles were obtained via a fast precipitation method as previously reported. Na_2CO_3 (0.1 M, 20 mL) and $\text{Ca}(\text{NO}_3)_2$ (20 mL, 0.1 M) solution were prepared by dissolving Na_2CO_3 and $\text{Ca}(\text{NO}_3)_2$ in PSS aqueous solution (10 mg mL^{-1}). Then Na_2CO_3 solution was rapidly poured into $\text{Ca}(\text{NO}_3)_2$ aqueous solution under magnetic agitation (1000 rpm), and the mixed solution was kept at 30 $^\circ\text{C}$ for 30 min, after which the formed vaterite CaCO_3 microparticles were washed with distilled water for 3 times and collected by centrifugation (3000 rpm).

HAP microparticles with a CaCO_3 core were formed by hydrothermal method. Briefly, 30 mL of Na_2HPO_4 solution (0.93 M) was added into the CaCO_3 microparticles. Then the mixture was transferred into 100 mL autoclave, sealed and heated to 140 $^\circ\text{C}$ for different period (3 h, 6 h and 12 h). The obtained HAP microparticles were washed with distilled water for 3 times and collected by centrifugation. Then, the formed HAP was employed as self-assembly template to fabricate hybrid HAP/CHI/HA hollow microparticles via LbL technique. The HAP was incubated in PSS/NaCl solution (1 mg mL^{-1} , pH 5.5) firstly to increase the electronegativity of HAP. Next, the HAP was incubated in CHI/NaCl solution (1 mg mL^{-1} , pH 5.5) for 10 min followed by a centrifugation-washing procedure for 3 times in NaCl solution (0.5 M, pH 5.5). Then the microparticles were incubated in HA/NaCl solution (1 mg mL^{-1} , pH 5.5) for 10 min followed by a centrifugation-washing procedure for 3 times in NaCl solution (0.5 M, pH 5.5). After self-assembly of 7 layers of polyelectrolyte and then removal of CaCO_3 cores with acetic acid

(0.1 M, pH 4.5), hollow HAP/CHI/HA (H-HAP/CHI/HA) hybrid microparticles were finally obtained. The H-HAP/CHI/HA microparticles formed by different hydrothermal reaction time (3, 6 and 12 h) were denoted as 3h-H-HAP/CHI/HA, 6h-H-HAP/CHI/HA and 12h-H-HAP/CHI/HA, respectively.

2.3 Characterization of H-HAP/CHI/HA hybrid microparticles

The surface morphology and particle size of the hybrid hollow microparticles were conducted with scanning electron microscopy (SEM, Philips-quanta-2000) at an accelerated voltage of 20 kV. The formation of H-HAP/CHI/HA hybrid microparticles was confirmed by means of energy dispersive X-ray spectrometer (EDX, EDAX). The high magnification morphology was observed using a field emission scanning electron microscope (FESEM, JEOL 7500F). The samples were spread homogeneously onto a silicon chip. When SEM observation, the silicon chip was stabilized on aluminum stubs and sputter coated with an approximate 100 Å layer of gold. TEM images were recorded on JEM-2100(UHR) emission electron microscope (FEI) with an accelerating voltage of 200 kV and the copper grid was used as the sample holder. FT-IR spectra were obtained on a Nicolet Protégé 460 FT-IR spectrometer in the range of 4000-500 cm^{-1} using a standard KBr disk technique. The phase characterization of microparticles was confirmed by X-ray power diffraction (XRD, PHILIPS X'Pert Pro diffractometer) using Cu-K α radiation ($\lambda=1.54178$ Å) with a graphite monochromator. Zeta-potential of the microparticles during the LbL self-assembly process was examined in NaCl solution (0.025 M, pH 5.5) by a Zeta-sizer (nano ZS90 Malvern Instruments). Each sample was measured at least 3 times and the average values were shown as resulting zeta-potential. Brunauer-Emmett-Teller (BET) analyses were used to calculate the specific surface area, pore size, and pore volume of the microparticles. Thermogravimetric analysis (TGA) was investigated by a TGA/DSC Simultaneous Thermogravimetric Analyzer (Diamond TG/DTA) with the heating rate of 10 $^{\circ}\text{C min}^{-1}$ under N_2 atmosphere.

2.4 Determination of drug encapsulation efficiency and *in vitro* release studies

40 mg of samples was added into 4 ml of DOX (0.5 mg mL^{-1})/NaCl solution. The suspension was stirred over 12 h under gentle shaking at 30 $^{\circ}\text{C}$. DOX loaded microparticles were obtained by washing with distilled water for 3 times. After being centrifuged, the DOX-loaded microparticles were dried in a vacuum oven at 40 $^{\circ}\text{C}$ for 24 h. The DOX amounts in the supernatant were established by UV-vis spectroscopy at 481 nm and calculated using a calibration curve. The DOX loading content and loading efficiency were calculated according to the following expressions:

$$\text{Drug content (mg per 10 mg sample)} = (\text{DOX fed} - \text{DOX in the supernatant}) / \text{microparticles amount} \times 10$$

$$\text{DOX loading efficiency (\%)} = (\text{DOX fed} - \text{DOX in the supernatant}) / \text{DOX fed} \times 100\%$$

For *in vitro* release test, the DOX-loaded microparticles were added into 50 mL of PBS (pH 7.4) or HCl solution (pH 2.1) under stirring in a shaking baths at 37 $^{\circ}\text{C}$. The medium (3 mL)

was periodically extracted at given time intervals and the withdrawn sample was replaced by the same volume of fresh medium. The amount of released drug was analyzed by UV-vis spectroscopy at 481 nm. All the tests were carried out in triplicate and the average values were shown in this study.

3. Results and Discussion

3.1 Characterization of H-HAP/CHI/HA microparticles

In the present work, PSS has been used as additive to prepare the vaterite CaCO_3 templates by the precipitation method.^{26,27} Carbonated HAP microparticles were then obtained via hydrothermal and dissolution-precipitation reaction using PSS-doped vaterite CaCO_3 as template.^{22,23} The HAP cores in this study are negatively charged because PSS is a negatively charged polyelectrolyte, which would improve the bonding force between HAP microparticles and polyelectrolytes.²⁶ In order to study the size, wall thickness and drug release property of H-HAP/CHI/HA hybrid microparticles thoroughly, four samples have been prepared in the present study: 3h-H-HAP/CHI/HA, 6h-H-HAP/CHI/HA, 12h-H-HAP/CHI/HA and 12h-H-HAP. 12h-H-HAP refers to the HAP microparticles with 12 h of hydrothermal reaction time and etched by acetic acid.

Fig. S1 shows SEM micrographs and corresponding EDX spectra of the samples during the different stage of hybrid microparticle preparation. The presence of P element in the EDX spectrum of HAP (B2) proved the formation of HAP. After 3 bilayers of CHI/HA were assembled, the HAP/CHI/HA hybrid microparticles (C1) were obtained. The hollow structure as shown in D1 indicated that the residuary CaCO_3 core was removed with acetic acid. The presence of N element coming from CHI in the corresponding EDX spectrum (D2) confirmed the successful adsorption of CHI/HA multilayers. The weakened Ca and distinct P signal demonstrated that CaCO_3 template was removed and HAP hollow structures could be successfully preserved after the etching procedure.^{26,27} The N_2 adsorption-desorption isotherms and corresponding pore size distribution curves of 3h-H-HAP microparticles are shown in Fig. S2. As illustrated in Fig. S2A, the isotherms of the H-HAP microparticles could be classified as type IV with a typical H1 hysteresis loop according to the IUPAC classification, indicating the presence of mesoporous structure. The Brunauer-Emmett-Teller (BET) surface area and total pore volume of H-HAP microparticles were calculated to be 113 $\text{m}^2 \text{g}^{-1}$ and 0.72 $\text{cm}^3 \text{g}^{-1}$, respectively. In addition, the Barret-Joner-Halenda (BJH) pore diameter of H-HAP microparticles was 25.01 nm as shown in Fig. S2B.

Fig. 3 shows SEM micrographs and the corresponding EDX spectra of 3h-H-HAP/CHI/HA, 6h-H-HAP/CHI/HA and 12h-H-HAP/CHI/HA hybrid microparticles. Partial structure collapse and capsule-like microparticles could be clearly observed, which might be due to the oppression of CHI/HA multilayers on HAP hollow structures. The corresponding EDX spectra (A3, B3 and C3) confirmed the presence of N element coming from CHI, indicating the successful adsorption of CHI/HA multilayers. It could be seen from Fig. 3 that the 3h-H-HAP/CHI/HA microparticles (A1 and A2) and 6h-H-HAP/CHI/HA microparticles (B1 and B2) had a distinct hollow interior, while the hollow structure of 12h-H-HAP/CHI/HA microparticles (C1 and C2) was

inconspicuous. The possible reason to this phenomenon is that the long period of hydrothermal reaction (12 h) has transformed most of CaCO_3 into HAP. Therefore, almost no CaCO_3 would be

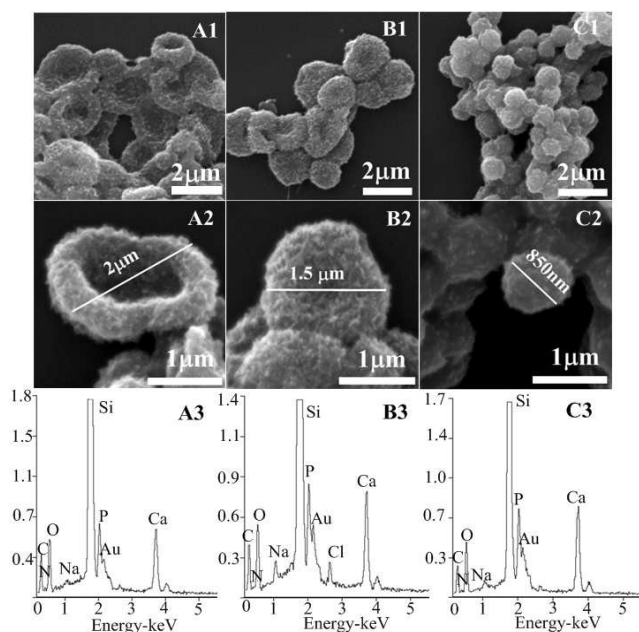


Fig. 3. SEM micrographs and corresponding EDX spectra of 3h-H-HAP/CHI/HA (A1, A2 and A3), 6h-H-HAP/CHI/HA (B1, B2 and B3) and 12h-H-HAP/CHI/HA (C1, C2 and C3) hybrid microparticles. 1 refers to low magnification, 2 refers to high magnification and 3 refers to EDX spectra, respectively.

dissolved during the etching procedure. It was also interesting to note from Fig. 3 that the particle size varied in the following order: 3h-H-HAP/CHI/HA > 6h-H-HAP/CHI/HA > 12h-H-HAP/CHI/HA. The diameter of 3h-H-HAP/CHI/HA microparticles was about 2 μm ; however, the value of 12h-H-HAP/CHI/HA ones decreased to about 850 nm. The possible reason to this phenomenon is that external nanoneedles around the HAP microparticles would be partially dissolved during the dissolution-precipitation reaction and the etching process, which resulted in the relatively small size of the hybrid microparticles. According to the high magnification FESEM image of the hybrid microparticles (Fig. 4), the external wall of HAP hollow microparticles were constructed by plenty of HAP nanoneedles (Fig. 4A). However, the surface of multilayer-coated microparticles (Fig. 4B) appeared smoother than that of the uncoated ones and the original nanopores seemed to be blocked, indicating the successful incorporation of CHI/HA multilayers around the HAP.^{27,37}

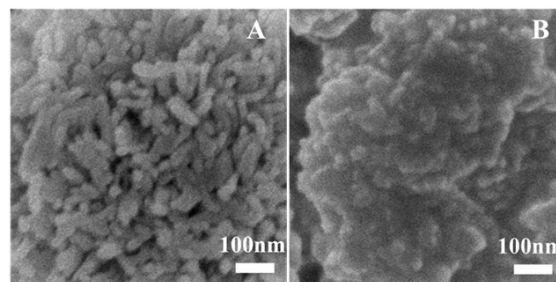


Fig. 4 The high magnification FESEM micrographs of 12h-H-HAP microparticles (A) and 12h-H-HAP/CHI/HA hybrid microparticles (B)

The hollow structure of the hybrid microparticles and the thickness variety of the particle shell were further confirmed by the TEM observation (Fig. 5). It could be observed that the hollow center was clearly observed in 3h-H-HAP/CHI/HA (A) and 6h-H-HAP/CHI/HA (B) microparticles, but the 12h-H-HAP/CHI/HA had a black center, which was similar to the results of Fig. 3. As discussed in Fig. 3, the CaCO_3 was almost converted completely to HAP after 12 h, therefore the 12h-H-HAP/CHI/HA microparticles were not hollow,^{20,21} as observed in Fig. 5C. In addition, the wall thickness of 3h-H-HAP/CHI/HA and 6h-H-HAP/CHI/HA were about 350 nm and 650 nm respectively. Under the hydrothermal reaction, the external wall of CaCO_3 templates was converted to HAP from the surface to the centre continuously.¹⁹ Therefore, after dissolving the CaCO_3 core, the thickness of HAP shell could be regulated via the adjustment of the hydrothermal reaction time as shown in Fig. 2. Fig. 6 shows the TEM images of 12h-H-HAP microparticles and 12h-H-HAP/CHI/HA hybrid microparticles. 12h-H-HAP microparticles had a loose solid structure. The nanoneedle-like HAP crystals could be clearly observed around the surface of H-HAP microparticles (B). However, nanoneedle-like HAP crystals were disappeared after the incorporation of CHI/HA polyelectrolyte inside the surface of H-HAP microparticles. It could be found that the surface of H-HAP/CHI/HA hybrid microparticles (C) became smoother and flatter than that of H-HAP ones (B), also confirming the successful incorporation of CHI/HA multilayers onto HAP microparticles.^{26,27}

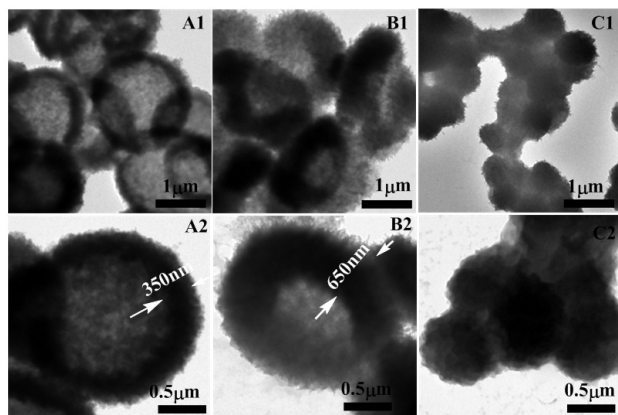


Fig. 5 TEM images of 3h-H-HAP/CHI/HA (A1 and A2), 6h-H-HAP/CHI/HA (B1 and B2) and 12h-H-HAP/CHI/HA (C1 and C2) hybrid microparticles. 1 refers to low magnification and 2 refers to high magnification.

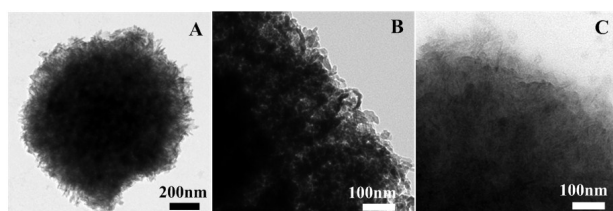


Fig. 6 The the low magnification TEM images of 12h-H-HAP microparticles (A), the high magnification TEM images of 12h-H-HAP (B) and 12h-H-HAP/CHI/HA hybrid microparticles (C).

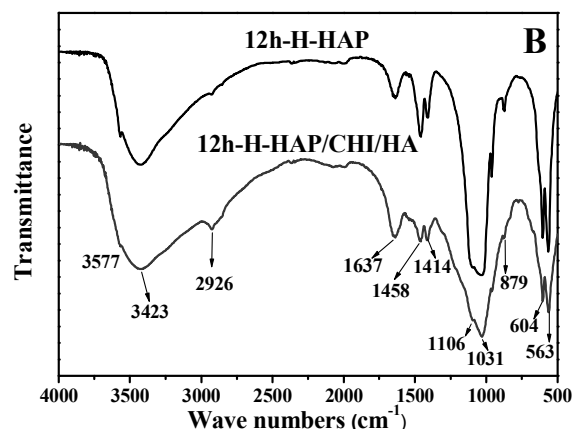
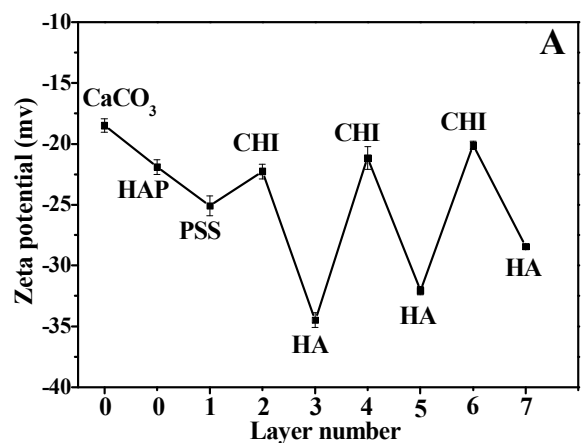


Fig. 7 Evolution of zeta-potential during deposition of (CHI/HA)₃ multilayer on the surface of HAP microparticles at pH 5.5 (A) and FT-IR spectra of 12h-H-HAP hollow microparticles and 12h-H-HAP/CHI/HA hybrid microparticles (B).

In this study, the CHI and HA were directly deposited on the HAP via the LbL self-assembly procedure. The LbL self-assembly process was monitored by the zeta-potential as shown in Fig. 7A. The zeta-potential of the PSS-doped CaCO₃ microparticles was around -18 mV because PSS was negatively charged. While the zeta-potential of HAP changed to -22 mV after hydrothermal reaction, which may be attributed to the partial moving of PSS to the surface of HAP microparticles from the CaCO₃ interior during the hydrothermal reaction process. The zeta-potential was around -20 mV for the outermost CHI layer and -30 mV for outermost HA layer. A clear zigzag-like pattern could be observed during the LbL self-assembly process. It should also be noted that the zeta-potential kept negative throughout the entire multilayer formation, which may be derived from the formation of hydrogen bonding between the amino groups of CHI and the carboxyl groups of HA.^{24,37} The functional groups in the 12h-H-HAP and 12h-H-HAP/CHI/HA microparticles have been characterized by FTIR spectroscopy, as shown in Fig. 5B. The absorption at 3577 cm⁻¹ derived from the hydroxyl group in HAP was not distinct owing to the overlapping with the broad peak of water (3423 cm⁻¹). The absorption peaks at 1031, 604 and 563 cm⁻¹ were corresponding to PO₄³⁻ and the characteristic peaks of B-type CO₃²⁻ were detected at 1458, 1414 and 879 cm⁻¹. In addition, the presence of absorption peak at

1106 cm^{-1} indicated that the samples were calcium deficient hydroxyapatite.^{38,39}

Fig. 8A presents the XRD patterns of 12h-H-HAP and 12h-H-HAP/CHI/HA hybrid microparticles. The characteristic HAP phases could be observed from the H-HAP/CHI/HA hybrid microparticles. It also be noted that faint CaCO_3 phases were observed from two samples because a little amount of CaCO_3 phases were remained in hybrid microparticles after the hydrothermal and dissolution-precipitation reaction process.^{23,40} TG analysis of 12h-H-HAP and 12h-H-HAP/CHI/HA microparticles (Fig. 8B) were performed to calculate the content of the CHI/HA polyelectrolyte in the hybrid microparticles. The weight loss curve of 12h-H-HAP/CHI/HA microparticles could be roughly divided into three steps. Dehydration below 150 °C was ascribed to the removal of adsorbed water. The mass loss at 450-800 °C was caused by the decomposition of the B- and A-type carbonate ions. In the range of 150-450 °C, a remarkable weight loss (12.88%) could be attributed to the polymer decomposition, indicating that the content of CHI/HA polyelectrolyte multilayer in hybrid microparticles was around 12.88% in weight.^{23,41}

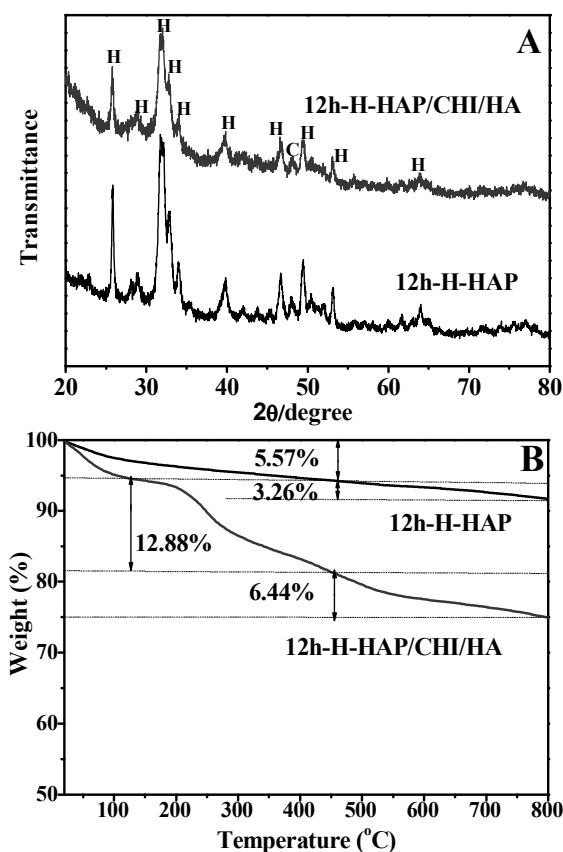


Fig. 8 XRD curves for 12h-H-HAP and 12h-H-HAP/CHI/HA hybrid microparticles (A), "C" denotes the CaCO_3 phase and "H" denotes the HAP phase. TG curves of 12h-H-HAP and 12h-H-HAP/CHI/HA hybrid microparticles (B).

3.2 DOX loading and sustained release

The H-HAP/CHI/HA hybrid microparticles with controllable size and wall thickness have the potential to be employed as the excellent drug vehicles with high drug loading efficiency and

controllable release properties. All prepared three samples showed relatively high drug loading efficiency around 80%, as illustrated in Table 1. It is clear that the inner hollow spaces and nanoplates or nanogranules inside hollow HAP microparticles improve the specific surface areas and then enhance the drug loading efficiency of the hybrid microparticles^{21,23}. At the same time, the negatively charged PSS in the hybrid microparticles could provide additional attractive forces for the positively charged DOX due to the electrostatic interaction between PSS and DOX. In addition, the polymer multilayers could partially obstruct the desorption of loaded drug from the H-HAP matrix, resulting the relatively high drug loading efficiency.

Table 1 Composition and drug loading efficiency of the samples

Sample	Compositions	Drug content (mg/10mg sample)	Loading efficiency (%)
1	3h-H-HAP/CHI/HA	0.376±0.091	84.1±2.8
2	6h-H-HAP/CHI/HA	0.346±0.089	83.5±1.1
3	12h-H-HAP/CHI/HA	0.312±0.022	73.8±3.0

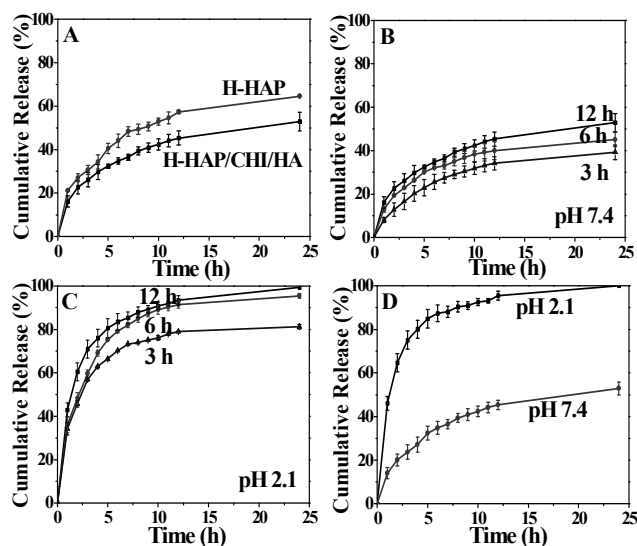


Fig. 9 DOX release profiles of 12h-H-HAP and 12h-H-HAP/CHI/HA microparticles at 37 °C and pH 7.4 (A). DOX release profiles at 37 °C from three H-HAP/CHI/HA hybrid microparticles at pH 7.4 (B) and pH 2.1 (C), pH-dependent release profiles of DOX from 12h-H-HAP/CHI/HA hybrid microparticles at 37 °C (D).

Fig. 9A shows the DOX release curves of 12h-H-HAP and 12h-H-HAP/CHI/HA hybrid microparticles at 37 °C and pH 7.4. The DOX release amount of 12h-H-HAP/CHI/HA microparticles within 24 h was 52%, whereas the value of 12h H-HAP microparticles was 65% with the same treatment. The sustained drug release property of 12h-H-HAP/CHI/HA hybrid microparticles is attributed to the introduction of compact CHI/HA multilayer. Polyelectrolyte multilayer shell acts as a barrier to obstruct the diffusion of loaded drug from the H-HAP matrix and then assuages the initial burst release of DOX.^{23,24} The DOX release profiles for the resulting hybrid microparticles with different hydrothermal reaction time at pH 7.4 and 2.1 are shown in Fig. 9B and C. The 3h-H-HAP/CHI/HA, 6h-H-HAP/CHI/HA and 12h-H-HAP/CHI/HA hybrid

microparticles exhibited the similar drug release trends at 37 °C and pH 7.4. During the first 4 h, all samples had a high release rate, but then reached the release equilibrium with increasing the release time. It was worth noting that the DOX release of the three samples exhibited the following trend whenever at pH 7.4 or 2.1: 12h-H-HAP/CHI/HA > 6h-H-HAP/CHI/HA > 3h-H-HAP/CHI/HA. This may be related to the porous structure of the hybrid microparticles and the thickness of the HAP wall. The mesopores of the hybrid microparticles act as the drug delivery channels. As demonstrated in Fig 5, 12h-H-HAP microparticles had the loosest HAP wall for the sake of the longest hydrothermal reaction time. On the other hand, the smallest size of 12h-H-HAP microparticles would make the encapsulated DOX release easily from the interior of the particles. Therefore, the drug release of 12h-H-HAP/CHI/HA microparticles is the highest among three samples.

3.3 pH-sensitive Release

The pH-sensitive release properties of the 12h-H-HAP/CHI/HA hybrid microparticles are shown in Fig. 9D. It could be observed that almost 99.9% of DOX were released at pH 2.1 over 24 h, but only 52.9% of DOX were released at pH 7.4 with the same treatment. The accumulative releasing amount of DOX reached 75% at pH 2.1 and 23% at pH 7.4 within 3h, respectively. Student's t-test analysis showed that the difference between the release of 12h-H-HAP/CHI/HA hybrid microparticles at pH 7.4 and 2.1 was extremely statistically significant (p value was 0.0001, greater than 95% confidence). The possible reason to the relatively high DOX release rate is the dissolution of HAP in the strong acidic solution as illustrated in Fig. 1.⁴¹⁻⁴³ On the other hand, most of the COO⁻ groups in HA ($pK_a = 3.0$) transform into COOH groups when the pH value decrease to 2.1, resulting the weakening of the electrostatic force between the CHI/HA polyelectrolyte⁴⁴. The cleavage of the electrostatic interaction makes the polyelectrolyte multilayer more permeable at pH 2.1, thus DOX could release rapidly.²³ In addition, the amino groups of CHI ($pK_a = 6.5$) are in the form of NH₃⁺ at pH 2.1, which generates the electrostatic repulsion between NH₃⁺ groups in CHI and the positively charged DOX molecules. It also accelerates the rapid diffusion of DOX at pH 2.1.

The *in vitro* drug loading and release results demonstrated that the prepared hybrid microparticles exhibited high drug loading efficiency, sustained and pH-dependent drug release properties. In addition, the size, wall thickness and drug release property of the resulting hybrid microparticles could be easily controlled via the adjustment of hydrothermal reaction condition. More importantly, no harmful organic solvent was involved during the preparation process. Therefore, the present paper provides a facile and green route to fabricate hierarchical environmentally friendly HAP-based drug carriers with controllable size, wall thickness and drug release property by combining natural polyelectrolyte and hollow HAP microparticles, which is highly attractive for drug delivery and smart bone regeneration area.

3.4 Drug release kinetics

In order to describe the kinetics of the drug release process from the controlled release, Korsmeyer–Peppas model was applied in the present study. The drug release kinetics was obtained by fitting the following standard empirical equation to

the experimental data.

$$M_t/M_\infty = kt^n \quad (1)$$

M_t is the amount of DOX released in time t , M_∞ the total amount of DOX in the matrix, k is the release constant for Korsmeyer–Peppas relating to the microparticles and n is the diffusion exponent characteristic of the release mechanism.⁴¹ For spherical drug carriers, if $0.43 < n < 0.85$, the drug release will be non-Fickian diffusion or anomalous transport. For $n < 0.43$, the drug delivery follows Fickian diffusion.^{45,46} The DOX release kinetics of the samples was summarized and the values of n , k , and correlation coefficient (R^2) obtained by curve-fitting are given in Table S1. The n values of 6h-H-HAP/CHI/HA and 3h-H-HAP/CHI/HA microparticles at pH 7.4 are 0.468 and 0.489, respectively. The results indicated that the non-Fickian transport was the dominated diffusion in the Release conditions. The rest samples in Table S1 were all lower than 0.43, indicating three samples had similar diffusion properties and the Fickian diffusion was the dominated diffusion mechanism at pH 2.1.

In order to deeply discuss the drug release kinetics of hybrid carriers, the n values were further determined from the slope of the $\ln(M_t/M_\infty)$ plot versus $\ln t$ at 37 °C for H-HAP/CHI/HA microparticles at pH 2.1 and 7.4 as shown in Fig. S3. The 3h-H-HAP/CHI/HA microparticles at pH 7.4 had the n values ranging from 0.829 to 0.546 (both higher than 0.43 and lower than 0.85, Fig. S3A), which suggested that the whole drug release process was due to non-Fickian transport. While the kinetics of drug release for other three samples all had a shift from non-Fickian to Fickian diffusion. The n values of the 12h-H-HAP/CHI/HA microparticles at pH 2.1 ranged from 1 to 0.424 and then changed to 0.204 (lower than 0.43), indicating a shift from Case-II transport to Fickian diffusion (Fig. S3B). The kinetics of drug release for the other two hybrid microparticles had the similar transformation trend at pH 2.1. This phenomenon may be attributed to the HAP dissolution and the corrosion of the CHI/HA multilayers at pH 2.1. This result indicated that the introduction of CHI/HA multilayer had changed the release kinetics of DOX and obstructed the diffusion of loaded drug into the solution.

The results demonstrate that we have developed a facile and green route to fabricate hierarchical drug carrier with controllable morphology and drug release property. In addition, the components of the prepared HAP/polyelectrolyte hybrid microparticles (HAP, hyaluronic acid and chitosan) all have good biodegradability, biocompatibility and lower toxicity. Therefore, the developed hollow HAP/polyelectrolyte hybrid microparticles show great potential as the novel drug carrier for controllable drug delivery or implanted artificial bone materials.

Conclusions

Hybrid HAP microparticles with a hollow HAP core and CHI/HA multilayer shell had been fabricated via hydrothermal method and the LbL self-assembly technique. The thickness of the HAP shell could be controlled via adjusting the hydrothermal reaction time and the size of the hybrid hollow microparticles varied between 850 nm and 2 μ m. The drug release results demonstrated that CHI/HA multilayers could potentially assuage the initial burst release of DOX from porous HAP matrix because the polymer multilayer shell acted as a barrier to control the

in-and-out of the drug. In addition, hollow HAP hybrid microparticles exhibited distinguished pH-dependent drug release property because of the weakening of electrostatic interaction between CHI/HA multilayers and the dissolution of porous HAP hollow core at acid condition.

Acknowledgements: This work was financially supported by the National Natural Science Foundation of China (Projects 20874090 and 21074119).

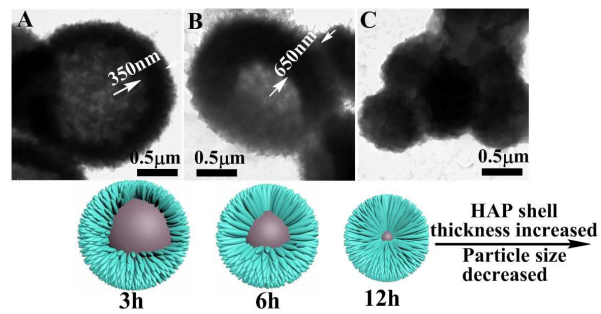
Notes and References

† School of Materials Science and Engineering, Zhengzhou University, Zhengzhou 450052, China

* Correspondence author: Jun Shi or Shaokui Cao (E-mail: shijun@zzu.edu.cn, caoshaokui@zzu.edu.cn)

†**Electronic Supplementary Information (ESI) available:** [SEM micrographs and corresponding EDX spectra of vaterite CaCO₃ cores, 6h-HAP, 6h-HAP/CHI/HA and 6h-H-HAP/CHI/HA microparticles. N₂ adsorption/desorption isotherms of 3h-H-HAP microparticles and the corresponding pore size distribution curves. Parameters *n*, *k* and *R*² determined by Korsmeyer–Peppas model for the DOX release of hybrid microparticles at different release conditions. Plots of ln(*M*_t/*M*_∞) versus ln *t* for the release profiles of hybrid microparticles at different pH values and temperatures].

- J. L. Arias and M. S. Fernández, *Chem. Rev.*, 2008, **108**, 4475–4482.
- S. Bhattacharyya, H. Wang and P. Ducheyne, *Acta. Biomater.*, 2012, **8**, 3429–34358.
- J. F. Shi, Y. J. Jiang, X. L. Wang, H. Wu, D. Yang, F. S. Pan, Y. L. Su and Z. Y. Jiang, *Chem. Soc. Rev.*, 2014, **43**, 5192–5210.
- S. H. Zhang, Z. Y. Jiang, W. Y. Zhang, X. L. Wang and J. F. Shi, *Biochem. Eng. J.*, 2015, **93** 281–288.
- L. C. Palmer, C. J. Newcomb, S. R. Kaltz, E. D. Spoerke, and S. I. Stupp, *Chem. Rev.*, 2008, **108**, 4754–4783.
- K. Pielichowska and S. Blazewicz, *Adv. Polym. Sci.*, 2010, **232**, 97–207.
- G. L. Wang, M. E. Babadađli and H. Uludađ, *Mol. Pharm.*, 2011, **8**, 1025–1034.
- A. Sinha, T. Mishra and N. Ravishankar, *J. Mater. Sci.: Mater. Med.*, 2008, **19**, 2009–2013.
- X. Y. Zhao, Y. J. Zhu, F. Chen, B. Q. Liu, C. Qi, J. Zhao and J. Wu, *Chem.-Asian J.*, 2013, **8**, 1306–1312.
- M. Vukomanović, S. D. Škapin, B. Jančar, T. Maksin, N. Ignjatović, V. Uskoković and D. Uskoković, *Colloids Surf. B*, 2011, **82**, 404–413.
- P. Yang, Z. Quan, C. Li, X. Kang, H. Lian and J. Lin, *Biomaterials*, 2008, **29**, 4341–4347.
- J. J. Guan, J. Yang, J. Q. Dai, Y. H. Qin, Y. Wang and Y. P. Guo, *RSC Adv.*, 2015, **5**, 36175–36184.
- M. Y. Ma, Y. J. Zhu, L. Li and S. W. Cao, *J. Mater. Chem.*, 2008, **18**, 2722–2727.
- F. Ye, H. F. Guo, H. J. Zhang and X. L. He, *Acta Biomater.*, 2010, **6**, 2212–2218.
- Y. Jiao, Y. P. Lu, G. Y. Xiao, W. H. Xu and R. F. Zhu, *Power Technol.*, 2012, **217**, 581–584.
- Q. Wu, C. Q. Liu, L. N. Fan, J. H. Shi, H. X. Jia, Q. Wu, L. W. Sun and F. H. Chen, *RSC Adv.*, 2013, **3**, 74860–7494.
- Y. P. Guo, T. Long, S. Tang, Y. J. Guo and Z. A. Zhu, *J. Mater. Chem. B*, 2014, **2**, 2899–2909.
- Y. S. Wang, Y. X. Moo, C. P. Chen, P. Gunawan and R. Xu, *J. Colloid Interf. Sci.*, 2010, **352**, 393–400.
- Q. F. Zhao, T. Y. Wang, J. Wang, L. Zheng, T. Y. Jiang, G. Cheng and S. L. Wang, *Appl. Surf. Sci.*, 2011, **257**, 10126–10133.
- C. Qi, Y. J. Zhu and F. Chen, *ACS Appl. Mater. Interfaces*, 2014, **6**, 4310–4320.
- Y. J. Guo, Y. Y. Wang, T. Chen, Y. T. Wei, L. F. Chu and Y. P. Guo, *Mater. Sci. Eng. C*, 2013, **33**, 3166–3172.
- Y. P. Guo, Y. B. Yao and Y. J. Guo, C. Q. Ning, *Micropor. Mesopor. Mater.*, 2012, **155**, 245–251.
- Y. P. Guo, Y. B. Yao, C. Q. Ning, Y. J. Guo and L. F. Chu, *Mater. Lett.*, 2011, **65**, 2205–2208.
- Y. S. Wang, M. S. Hassan, P. Gunawan, R. Lau, X. Wang and R. Xu, *J. Colloid Interface Sci.*, 2009, **339**, 69–77.
- F. Ye, H. F. Guo, H. J. Zhang and X. L. He, *Acta Biomater.*, 2010, **6**, 2212–2218.
- D. S. Feng, J. Shi, X. J. Wang, L. Zhang and S. K. Cao, *RSC Adv.*, 2013, **3**, 24975–24982.
- S. H. Xu, J. Shi, D. S. Feng, L. Yang and S. K. Cao, *J. Mater. Chem. B*, 2014, **2**, 6500–6507.
- S. F. M. V. Dongen, H. P. M. D. Hoog, R. J. W. Peters, M. Nallani, R. J. M. Nolte and J. C. M. V. A. V. Hest, *Chem. Rev.*, 2009, **109**, 6212–6274.
- J. Borges and J. F. Mano, *Chem. Rev.*, 2014, **114**, 8883–8942.
- U. Manna and S. Patil, *Langmuir*, 2009, **25**, 10515–10522.
- D. B. Shenoy, A. A. Antipov, G. B. Sukhorukov and H. Möhwald, *Biomacromolecules*, 2003, **4**, 265–272.
- S. Vasiliu, M. Popa and M. Rinaudo, *Eur. Polym. J.*, 2005, **41**, 923–932.
- R. C. Polexe and T. Delair, *Molecules*, 2013, **18**, 8563–8578.
- G. Berth, A. Voigt, H. Dautzenberg, E. Donath and H. Möhwald, *Biomacromolecules*, 2002, **3**, 579–590.
- W. E. Krause, E. G. Bellomo and R. H. Colby, *Biomacromolecules*, 2001, **2**, 65–69.
- K. Kakehia, M. Kinoshita and S. I. Yasueda, *J. Chromatogr. B*, 2003, **797**, 347–355.
- C. Du, J. Shi, J. Shi, L. Zhang and S. K. Cao, *Mater. Sci. Eng., C*, 2012, **33**, 3745–3752.
- D. Walsh, T. Furuzono and J. Tanaka, *Biomaterials*, 2001, **22**, 1205–1212.
- J. Shi, J. Shi, C. Du, Q. Chen and S. K. Cao, *J. Membr. Sci.*, 2013, **433**, 39–48.
- D. Li, J. M. He, W. L. Cheng, Y. D. Wu, Z. Hu, H. Y. Tian and Y. D. Huang, *J. Mater. Chem. B*, 2014, **2**, 6089–6096.
- J. M. Lee and H. S. Yun, *J. Mater. Chem. B*, 2014, **2**, 1255–1263.
- J. Shi, W. Y. Qi, G. F. Li and S. K. Cao, *Mater. Sci. Eng. C*, 2012, **32**, 1299–1306.
- Y. H. Yang, C. H. Liu, Y. H. Liang and F. H. Lin, *J. Mater. Chem. B*, 2013, **1**, 2447–2450.
- Y. J. Zhu and F. Chen, *Chem.-Asian J.*, 2015, **10**, 284–305.
- P. L. Ritger and N. A. Peppas, *J. Controlled Release*, 1987, **5**, 37–42.
- G. Schliecker, C. Schmidt, S. Fuchs, A. Ehinger, J. Sandow and T. Kissel, *J. Controlled Release*, 2004, **94**, 25–37.



Hollow hydroxyapatite/polyelectrolyte microparticles with controllable size, wall thickness and drug delivery property have been fabricated via green hydrothermal method and LbL self-assembly technique.